How to cite: Angew. Chem. Int. Ed. 2024, e202420572
doi.org/10.1002/anie.202420572

Porphyrinoids

Coordinative Self-assembly of π-Electron Magnetic Porphyrins

María Tenorio[+], Marco Lozano[+], Lenka Cerna, Miguel Martínez García, Maxence Urbani, Koen Lauwaet, Kalyan Biswas, Diego Soler-Polo, Shanmugasibi K. Mathialagan, Sofía O. Parreiras, José M. Gallego, Rodolfo Miranda, José Ignacio Urgel, Tomás Torres,* Pavel Jelínek,* Giovanni Bottari,* and David Écija**

Abstract: π-Electron magnetic compounds on surfaces have emerged as a powerful platform to interrogate spin interactions at the atomic scale, with great potential in spintronics and quantum technologies. A key challenge is organizing these compounds over large length scales, while elucidating their resulting magnetic properties. Herein, we offer a relevant contribution toward this objective, which consists of using on-surface synthesis coupled with coordination chemistry to promote the self-assembly of π-electron magnetic porphyrin species. A porphyrin precursor equipped with carbonitrile moieties in a *trans* arrangement was prepared by solution synthesis and deposited on Au(111)/mica. Depending on the specific growth protocol, surface-promoted reactions led to the transformation of the precursor into non-magnetic Au-CN coordinated porphyrin monomers, covalent porphyrin dimers, and one-dimensional porphyrin polymers (based on porphyrin monomers or covalent porphyrin dimers), as revealed by scanning probe microscopy studies combined with theoretical calculations. Interestingly, the scanning tunneling microscopy tip could convert such closed-shell porphyrin units into open-shell species by the removal of some peripheral hydrogen atoms. The magnetic features (i.e., singlet or triplet ground state) of the porphyrin units comprising the polymers were investigated for polymers of different lengths. No magnetic exchange coupling between adjacent units was observed, suggesting protection of the magnetic entities.

Introduction

The study of π-electron magnetism in molecular and polymeric compounds is a young and promising research field, which has blossomed triggered by the unique magnetic properties these systems present. For example, such nano-architectures exhibit weak spin-orbit and hyperfine couplings, resulting in longer relaxation times and reduced decoherence of electron spins,[1–4] features that have prompted the use of π-electron magnetic organic nano-structures for spintronics and quantum information applications.[5] However, despite such great potential, the inherent high reactivity presented by π-electron magnetic architectures, which arises from their radical nature, poses an important limitation to their effective preparation.[3]

Recently, on-surface synthesis has emerged as a powerful strategy to fabricate and characterize at the atomic scale open-shell carbon-based nanomaterials. In this context, it is worth pointing out to the seminal works on graphene nanoribbons junctions[6] and distinct families of graphene

[*] M. Tenorio,[+] L. Cerna, M. Martínez García, M. Urbani, K. Lauwaet, K. Biswas, S. K. Mathialagan, S. O. Parreiras, R. Miranda, J. I. Urgel, T. Torres, G. Bottari, D. Écija
Instituto Madrileño de Estudios Avanzados en Nanociencia (IMDEA Nanoscience), 28049 Madrid, Spain
E-mail: maria.tenorio@imdea.org
tomas.torres@uam.es
giovanni.bottari@uam.es
david.ecija@imdea.org

M. Lozano,[+] D. Soler-Polo, P. Jelínek
Institute of Physics, Academy of Sciences of the Czech Republic, CZ 16200 Prague, Czech Republic
E-mail: jelinekp@fzu.cz

J. M. Gallego
Instituto de Ciencia de Materiales de Madrid (ICMM), CSIC, Cantoblanco, 28049 Madrid, Spain

R. Miranda
Departamento de Física de la Materia Condensada and Condensed Matter Physics Center (IFIMAC), Universidad Autónoma de Madrid, Cantoblanco, 28049 Madrid, Spain

M. Martínez García, T. Torres, G. Bottari
Departamento de Química Orgánica, Universidad Autónoma de Madrid, 28049 Madrid, Spain

P. Jelínek
Regional Centre of Advanced Technologies and Materials, Czech Advanced Technology and Research Institute (CATRIN), Palacký University Olomouc, Olomouc 78371, Czech Republic

T. Torres, G. Bottari
Institute for Advanced Research in Chemical Sciences (IAdChem), Universidad Autónoma de Madrid, 28049 Madrid, Spain

[+] These authors have contributed equally.

fragments such as triangulenes,[7–13] Clar's goblet,[14] periacenes,[15,16] zethrenes,[17,18] and rhombenes.[19,20]

Among the molecular building blocks that could be used to promote the formation of π-electron magnetic structures on surfaces, porphyrins are particularly interesting platforms due to their planar structure and high chemical stability, the presence of an extended π -surface, and the possibility to incorporate paramagnetic atoms in their central cavity. While few examples of open-shell porphyrins prepared by solution synthesis have been reported to date, either as monomeric species[21] or π-fused porphyrin oligomers,[22] important stability issues are often encountered for such open-shell conjugates due to their high chemical reactivity. More recently, to overcome this limitation on-surface synthesis has been used as a strategy to prepare open-shell porphyrin monomers[23] and nanotapes[24] directly on metal surfaces. Species which were further characterized both from the structural and electronic point of view by using scanning probe microscopy techniques.

While important advances have been made in the preparation and characterization of surface-supported π-electron magnetic nanostructures, an important issue that deserves more attention is the possibility to organize them over multiple length scales, something which would prompt the incorporation of such systems in devices.

In the last three decades, many supramolecular and covalent protocols have been employed in order to promote the formation of surface-confined periodic and quasiperiodic nanostructures.[25–32] A particularly powerful strategy to fabricate one-dimensional (1D) and two-dimensional (2D) nanostructures relies on the use of metal-ligand coordination chemistry, employing a wide variety of metal atoms including alkali, d-block transition metals, and lanthanide elements.[26,27] However, concerning π-electron magnetic compounds, the knowledge about their ordering on surfaces is extremely limited,[32,33] being the potential of coordination chemistry underexplored. Two main questions emerge while coordinating a magnetic compound to a metal atom. First, what is the influence of such coordination on the "uncomplexed" magnetic ground state features of the compound. Second, and crucial for any potential application, whether a magnetic exchange can be established between monomers, as previously found for covalent nanoarchitectures based on magnetically-active monomers,[32–34] or, on the contrary, the magnetic entities do not interact with each other.

Herein, we present a comprehensive study including scanning probe microscopy and spectroscopy, complemented by theoretical simulations, to assess such questions by preparing metal-organic porphyrin polymers, which units feature an open-shell character. To this aim, the deposition on Au(111)/mica of a porphyrin monomer equipped with carbonitrile moieties in a *trans* arrangement, results upon thermal stimulus in the formation of two types of 1D metal-organic polymers featuring monomeric porphyrin or laterally-fused covalent porphyrin dimers coordinated by gold atoms. Upon subsequent tip-induced dissociation of two hydrogen atoms, the monomeric and laterally-fused porphyrin units are transformed into open-shell species which do not display interunit magnetic exchange interaction, thus, preserving the magnetic character of the constituent entities.

Our study shows the possibility of fabricating and characterizing complex nanoarchitectures comprising magnetic entities by using a synergic effort comprising on-surface covalent synthesis and coordination chemistry. Specifically, we exemplify the potential of surface-confined coordination chemistry to direct the periodic assembly of diradical porphyrin monomers, giving rise to the formation of 1D coordination polymers, while preventing the magnetic exchange coupling between spins from adjacent building units, a finding of relevance for quantum information. Altogether, our results pave the way for the use of self-assembly to drive the organization of multiradical and π-electron magnetic nanostructures on surfaces and the consequent implications on their magnetic properties.

Results and Discussion

The fabrication of the target porphyrin-based metal-organic nanostructures starts with the solution synthesis of **1**, a porphyrin equipped at its *trans meso* positions with two 4-cyano-2,6-dimethyl phenyl moieties (see Supporting Information, section 2 for details). Derivative **1** is then deposited on Au(111)/mica under ultra-high vacuum (UHV), and the sample annealed using two different protocols. The deposition of **1** on Au(111)/mica substrate held at 300 °C gives rise to the formation of discrete dihydrogenated porphyrin monomers (**Por HM**) ($n=1$) as well as polymeric dihydrogenated porphyrin nanochains (**1D Por HNC**) ($n>1$) (Scheme 1, red arrow) (Figure 1a).

Por HM features two phenalenyl-fused fragments, each of them sustaining a carbonitrile group coordinated to a gold adatom as well as two sp^3 carbon atoms at the former porphyrin β positions (see below).[23,35,36] It is worth noticing here that, although the surface-promoted intramolecular oxidative ring-closure reaction of **1**, in theory, should lead to the formation of a diradical porphyrin monomer (**Por M**) (or its analogue not coordinated to gold adatoms), such species is not observed in these experimental conditions. This result could be rationalized considering that the highly reactive character of **Por M** favours its reaction with residual hydrogen atoms (most probably resulting from the oxidative cyclodehydrogenation process itself) leading to the formation of the dihydrogenated species **Por HM**.[23,33,37] While our STM analysis of **Por HM** does not allow to unequivocally determine the exact position of the two CH_2 on the porphyrin edge, taking into account previous works on phenalenyl-fused porphyrin derivatives analogous to the one reported here,[23a,33] the most probable regioisomer is the one having the two CH_2 at two β porphyrin positions located in a "*trans*" relative arrangement, at opposite sides with respect to the porphyrin longer axis (i.e., **Por HM** in Scheme 1). For a more detailed explanation of the possible regioisomers of **Por HM** see Section 4 of the Supporting Information. However, these extra hydrogens in **Por HM** can be dissociated via tip manipulation (Figures 1b–d). On the other hand, if **1** is deposited on Au(111)/mica kept at room

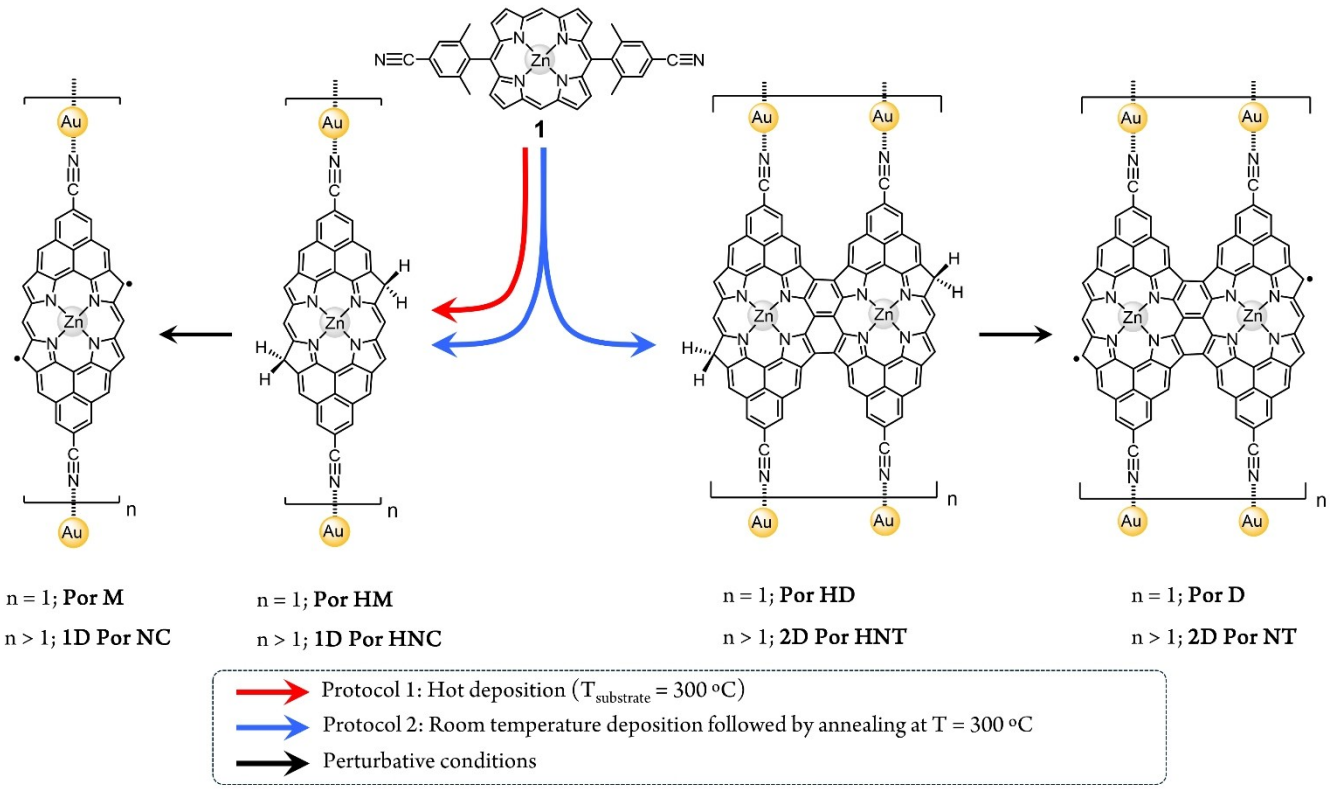

Scheme 1. Formation of one-dimensional coordination polymers based on diradical porphyrins on Au(111)/mica.

temperature, and the substrate subsequently annealed to 300 °C for 60 minutes, triply fused porphyrin nanotapes[38] coordinated by gold atoms are found (i.e., **1D Por HNT**) together with **1D Por HNC** (Scheme 1, blue arrows). No **1D Por HNT** polymers comprising laterally fused porphyrin trimers or longer oligomers as units were observed probably due to the rapid passivation of the laterally fused porphyrin dimers by residual hydrogen atoms. In analogy to the product **1D Por HNC**, **1D Por HNT** can be dehydrogenated by either scanning at perturbative conditions or by applying bias sweeps that afford **1D Por NT**.

An overview scanning tunneling microscopy (STM) image of the deposition of **1** on Au(111)/mica substrate held at 300 °C shows 1D polymers of different lengths (i.e., from few porphyrin units to long polymers) following the FCC paths of the herringbone reconstruction (Figure 1a). All 1D polymers display rounded features at the porphyrin edges which are assigned to gold adatoms coordinated to the porphyrin entities through the carbonitrile functional groups (Figure 1b).[39–41]

While coordination chemistry on surfaces has already displayed that carbonitrile-gold coordination on Au(111) usually results in a triply-coordinated motif,[39–41] **1D Por HNC** shows instead a doubly-coordinated geometry. Notably, in **1D Por HNC** and **Por HM**, the carbonitrile-gold atom bond strength, considered high in STM break junctions and, thus, used as an anchoring system,[43] is sufficiently strong not to break during the interaction with the STM tip (Figures 1b and S14).

In order to induce an open-shell character in **Por HM**, we used tip-induced manipulation[23,33,37] either applying bias sweeps, typically from 1.5 V to 2.5 V (i.e., feedback loop open, 10 pA) until a step in current was detected, or by scanning at perturbative conditions (i.e., 2.3 V and 200 pA). Figure 1c illustrates the stepwise dehydrogenation procedure of a porphyrin unit within a polymer comprising seven monomers (i.e., **1D Por HNC** with $n = 7$), affording sequentially singly (middle panel of Figure 1c) and doubly dehydrogenated porphyrin monomers (right panel of Figure 1c). This protocol can be successfully performed independently from the length of the target **1D Por HNC**, as exemplified in Figures 1d–g. The singly and doubly dehydrogenated porphyrins, which present one and two unpaired electrons, respectively, are expected to show magnetic features, which can be monitored by imaging at low bias and performing scanning tunneling spectroscopy (STS) close to zero bias.[23,37,43] Figure 2 shows a sequence of tip-induced hydrogen dissociation for a **Por HM** species, which in its pristine configuration does not show any STS fingerprint close to zero bias (Figure S15). After the first bias sweep, two effects are observed. On the one hand, there is the enhancement of the local density of states while imaging at 5 mV at the porphyrin rim where the hydrogen dissociation has taken place (Figure 2a). On the other hand, a resonance at zero bias resonance appears (Figure 2e). Both features can be attributed to the Kondo effect between the tip-induced radical located at the porphyrin rim and the Au(111) surface.[35,36,37] A second bias sweep at the remaining sp^3

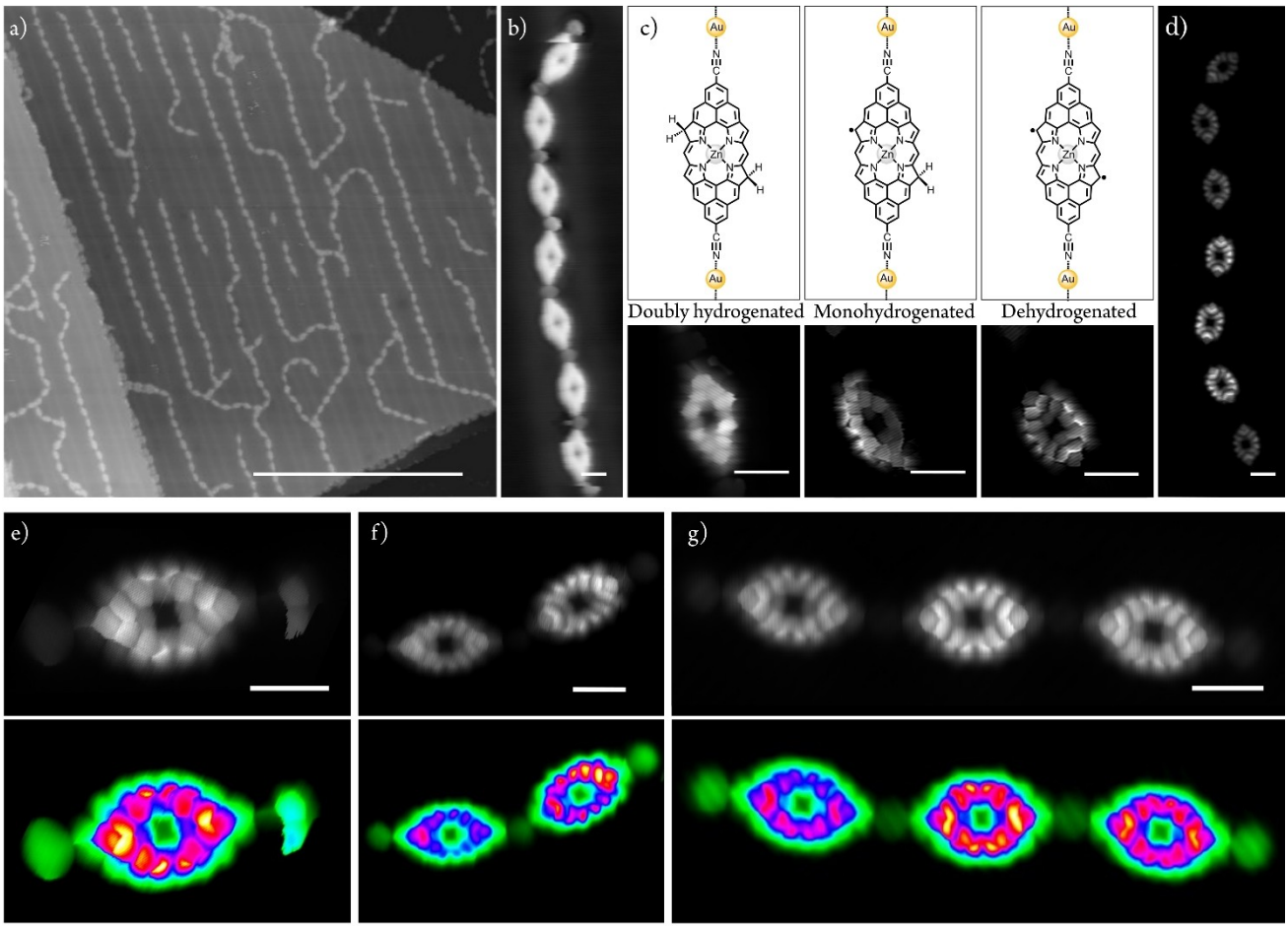

Figure 1. On-surface synthesis of **Por HM** and **1D Por HNC** on Au(111)/mica and their transformation into **Por M** and **1D Por NC**. a) Representative overview STM image of 1D metal-organic polymers **1D Por HNC** obtained after depositing a submonolayer amount of **1** on a Au(111)/mica substrate held at 300 °C. b) Close view STM image at constant current of a polymer comprising seven monomers, **1D Por HNC**. c) Chemical structure (above) and STM image (below) at constant height of the tip-induced dehydrogenation sequence of a Por unit within **1D Por HNC** in b). d) Constant height STM image after performing tip-induced dehydrogenation of all the Por units in polymer **1D Por HNC** depicted in b), affording **1D Por NC**. e–g) STM constant height images of e) **Por M**, and f) two-member and g) three-member polymer **1D Por NC**. Images are duplicated and displayed with different color palettes in order to highlight either the molecular structure or the coordinating gold adatoms. Additionally, constant height STM images with 'PseudoColor' palette (bottom) have the chemical structure superimposed. All STM images are acquired with a CO-functionalized tip. Scanning parameters: a) 100 mV, 20 pA; b) 100 mV, 20 pA; c) 20 mV, 100 pA, Z-offset (from left to right): −200 pm, −625 pm, −353 pm; d) 10 mV, 20 pA, Z-offset: −500 pm; e) 10 mV, 50 pA, Z-offset: −55 pm; f) 10 mV, 20 pA, Z-offset: 0 pm; g) 10 mV, 10 pA, Z-offset: 280 pm;. Scale bars: a) 50 nm, b)-c) 1 nm, d) 5 nm, e–g) 1 nm. Positive and negative Z-offset values stand for further or closer tip-sample distance from the set point conditions, respectively.

carbon atom of the porphyrin removes the other hydrogen, affording **Por M** (Figure 2b). Such hydrogen dissociation event is clearly detected by STS, which shows two step-like peaks, symmetrically located around zero bias, being tentatively assigned to a singlet-triplet spin excitation (blue plot in Figure 2f), as previously encountered in other molecular species featuring π-electron magnetism, and due to the exchange coupling between unpaired electrons.[3,6,14,20,35,37,43] By performing d^2I/dV^2 spectroscopy on **Por M**, the magnetic exchange coupling energy is recorded obtaining a value of $J = 26$ mV (green plot in Figure 2f).

We performed Density Functional Theory (DFT)[44] and Complete Active Space Configuration Interaction (CASCI)[45] calculations to elucidate the role of metal-ligand coordination on the magnetic properties of **Por M** (see Supporting Information for details). Firstly, we optimized the geometry of **Por M** on Au(111) using periodic DFT slab calculations. Such geometry, illustrated in Figure S16, reveals that the coordinative gold adatoms are not on the same plane as the porphyrin core, being closer to the surface. Generally, the single electron DFT simulations fail to describe correctly the electronic structure of open-shell polyradical systems. To afford many-body CASCI calculations, we built a cluster model from the optimized DFT geometry on Au(111) surface. We intentionally passivated gold adatoms of **Por** monomer with hydrogens to mimic their covalent bond to the substrate (see discussion in Supporting Information and Figures S17 and S18). Our cluster CASCI(14,14) simulations, including 14 electrons in 14 molecular orbitals in the active space, indicate an open-

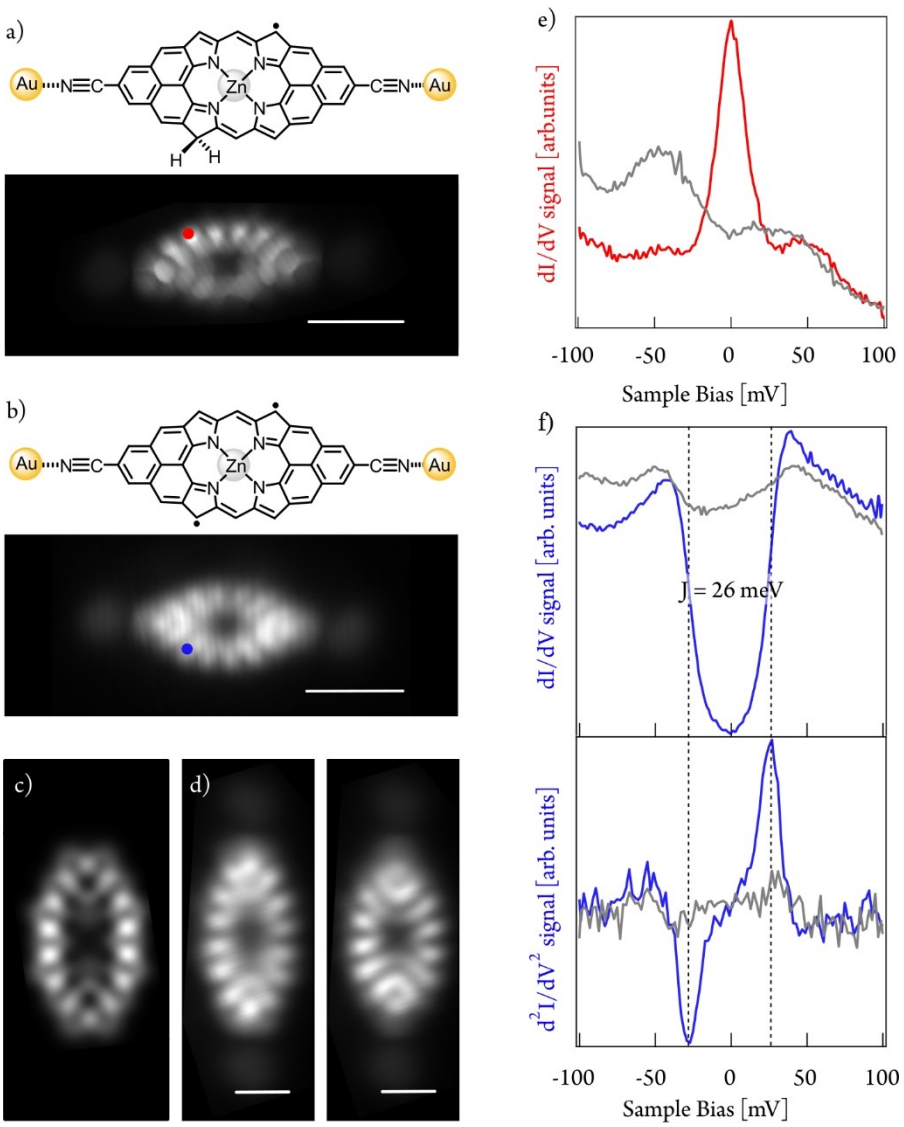

Figure 2. Formation of **Por M** by tip-induced hydrogen dissociation of **Por HM** and subsequent electronic characterization of the species. a,b) Chemical structure (top panels) and corresponding constant height STM images (bottom panels) of a) monohydrogenated **Por HM** and b) **Por M**. Scanning parameters: a) 5 mV, 10 pA, Z-offset: 130 pm; b) 5 mV, 10 pA, Z-offset: 540 pm. Scale bars = 2 nm. c) Simulated dI/dV map of **Por M** for the singlet-triplet transition (see Figure S19 for further discussion); d) Experimental dI/dV maps at constant current acquired at −25 mV (left image) and +25 mV (right image). $V_{modulation}$ = 5 mV. Scanning parameters: −25 mV/25 mV, 100 pA, Z-offset: 420 pm. Scale bars = 1 nm. e) and top panel f) dI/dV spectroscopy at selected points indicated by red and blue dots on the STM images a) and b), respectively. $V_{modulation}$ = 3 mV. Bottom panel f) d^2I/dV^2 spectroscopy at same selected points as top panel f). d^2I/dV^2 maximum and minimum are at −26 mV and +26 mV, respectively.

shell singlet ground state of **Por M** and the first excited triplet state at 78 meV. The singlet-triplet energy difference is further decreased to 15 meV if we include the dynamical correlation corrections using N-Electron Valence Perturbation Theory (NEVPT2).[46,47] Next, we calculated the Natural Transition Orbitals (NTO)[48] corresponding to the singlet-triplet transition (Figure S19). Figure 2c displays a simulated dI/dV map of **Por M** corresponding to the combination of the NTO orbitals using PP-STM code,[49] which nicely matches with the experimental dI/dV maps acquired at ±26 mV (Figure 2d). Here, it is important to point out that theoretical CASCI(14,14) calculations suggest that, in the gas phase, a planar configuration of **Por M** results in a triplet ground state, as previously encountered for an analogous porphyrin lacking the two carbonitrile functional groups.[23] However, due to the out-of-plane arrangement of the carbonitrile-gold coordination, the ground state becomes the open-shell singlet (see discussion in section 8 of the Supporting Information).

Figure 3 shows the short-range STS of a three-member porphyrin polymer (i.e., **1D Por NC**, n = 3) after double dehydrogenation of each porphyrin unit by tip-induced manipulation (see full sequence in Figure S20). The interaction of unpaired electrons on each porphyrin unit displays

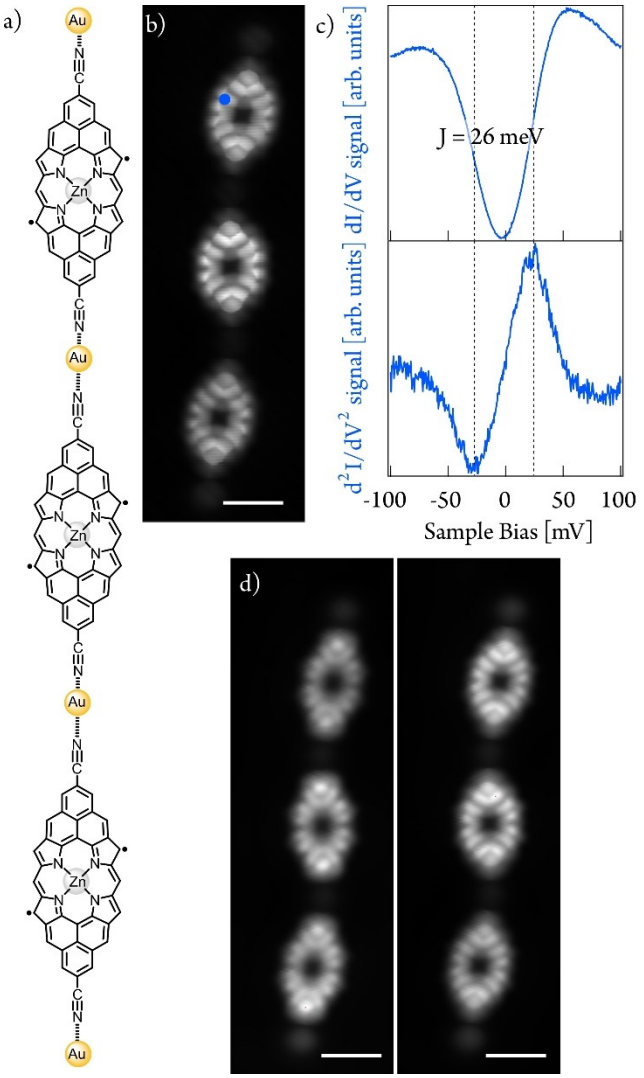

Figure 3. Electronic characterization at low energies of a three-member **1D Por NC**. a) Chemical structure and b) STM image at constant height of a three-member **1D Por NC**. Scanning parameters: 10 mV, 10 pA, Z-offset: 280 pm. Scale bar = 1 nm. c) d*I*/d*V* (blue plot) and d^2I/dV^2 (green plot) spectroscopy on a porphyrin unit within three-member **1D Por NC** at the position indicated by the blue dot in b). d^2I/dV^2 maximum and minimum are at −26 and +26 mV, respectively. d) d*I*/d*V* maps acquired at −25 mV (left image) and +25 mV (right image). $V_{modulation}$ = 5 mV. Scanning parameters: −25 mV/25 mV, 20 pA, Z-offset: 300 pm.

an exchange interaction energy of around 26 mV, a value identical to that observed for individualized **Por M** species (see above). Additionally, the structural parity of the polymer does not affect this exchange interaction (see in Figure S21 the electronic characterization of a two-member porphyrin polymer).

Moreover, we performed long-range STS experiments to identify the frontier orbitals and determine the band gaps of **1D Por NC**. Regardless of the length of the metal-organic porphyrin polymer investigated, onsets at –0.3 and +0.5 V are observed, which we tentatively identify as the singly occupied molecular orbital (SOMO) and singly unoccupied molecular orbital (SUMO), respectively, thus inferring a band gap of 0.8 eV. In fact, the experimental d*I*/d*V* maps at those resonances reasonably agree with the simulated ones in the gas phase (Figure S22), thus corroborating our reasoning behind the experimental results. Herein, it is important to highlight that no band-shift or change in the band gap are observed for 1D porphyrin polymers of different length, with just minute variations, which suggests that the porphyrin units could be considered as individual entities from the electronic and magnetic point of view.

Next, we turn our attention to the side reaction pathway depicted in the right panel of Scheme 1 (i.e. the formation of **1D Por HNT**). Such pathway can be favoured, though always giving **1D Por HNT** as the minor species, if **1** is deposited at room temperature and then post-annealed to 300 °C for long annealing times (i.e., 60 minutes). Such conditions allow for the lateral coupling of diradical porphyrin monomers giving rise to triply-fused porphyrin dimers which are then linked between them by CN–Au metal-ligand interactions. It is interesting to note that 1D polymers comprising laterally-fused porphyrin trimers or oligomers were not observed probably due to a rapid hydrogenation of the highly-reactive diradical porphyrin dimers. This process hampers their further lateral growth.

Stepwise hydrogen dissociation to form a **Por D** unit within a **1D Por HNT** segment and its corresponding short-range STS characterization is displayed in Figures 4b–d. The fully-passivated unit does not show any significant magnetic feature, pointing out to its close-shell character (Figure 4b, bottom). First hydrogen dissociation at one of the two terminal positions of a triply-linked porphyrin dimer within the nanotape gives rise to the emergence of a resonance at zero bias resonance (Figure 4c, bottom), which is rationalized as a Kondo effect due to the presence of a radical which interacts with the underneath Au(111) surface, in analogy to what seen for the singly dehydrogenated **Por HM** species (see above). Upon removal of a second hydrogen on the remaining sp^3 carbon atom of the targeted porphyrin dimer, a zero-energy bias resonance at each rim of the porphyrin is detected (Figure 4d, bottom).[36]

To rationalize the latter experimental observation, we adopted a similar theoretical procedure as in the case of porphyrin **M**. First, we optimized the geometry of **Por D** on the Au(111) surface (Figure S23) using the DFT slab calculations. Next, we adopted a cluster model derived from the optimized DFT slab structure with passivated Au atoms by hydrogen atoms (Figures S24 and S25). Our cluster NEVPT2/CASCI(12,12) calculations of **Por D** reveal a triplet ground state. To support the presence of Kondo screening, we performed a theoretical analysis of the Kondo screening process using the multi-orbital Anderson impurity model.[50] We found two dominant screening channels with antiferromagnetic (AFM) coupling that rationalized the presence of the Kondo screening. Figure 4e shows the Kondo orbitals[48] associated with the AFM screening channel and the corresponding simulated d*I*/d*V* map (Figure 4f). Good agreement between the simulated d*I*/d*V* map of the Kondo orbital and the experimental STM image acquired at low bias energy (Figure 4g) indicates the

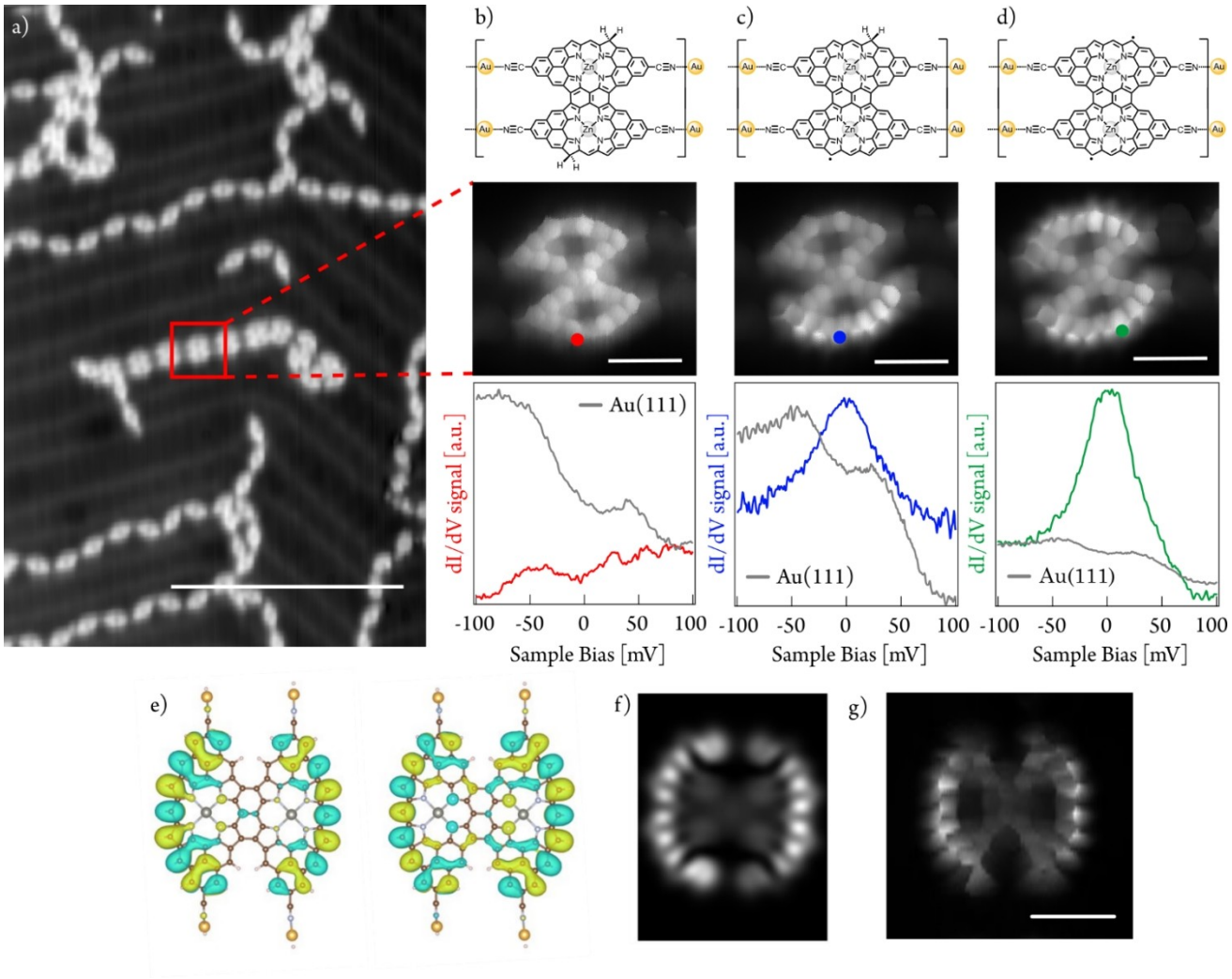

Figure 4. Structural and electronic characterization of **1D Por HNT** on Au(111)/mica and the tip-induced transformation of a constituent unit into **Por D**. a) Overview STM image showing a region featuring few **1D Por HNT** in coexistence with predominant **1D Por HNC** species obtained after depositing a submonolayer coverage of **1** on Au(111)/mica. Scanning parameters: $V_{bias} = 100$ mV, $I_t = 20$ pA. Scale bar = 20 nm. b–d) Chemical structure (top panel), STM image at constant height (medium panel), and d*I*/d*V* spectroscopy (bottom panel) of b) fully dihydrogenated porphyrin dimer unit within **1D Por HNT** (marked with a red frame in a), c) subsequent monohydrogenated species from b) obtained by bias sweeps, and d) fully dehydrogenated porphyrin dimer within **1D Por HNT**. Red, blue and green dots on the constant height images depict the position of spectra acquisition. b–d) Scale bar = 2 nm. b–d). Scanning parameters: 10 mV, 50 pA, Z-offset: 380 pm. The final graph is an average of three-point spectra; e) Kondo orbitals of the two antiferromagnetic channels; f) Simulated d*I*/d*V* map given by the linear combination of e) corresponding to the spatial distribution of the Kondo signal at zero bias resonance; g) Constant-height STM image of a **1D Por NT** at 5 mV (Kondo map). Scanning conditions: 5 mV, 16 pA, Z-offset: 0 pm. Scale bar = 1 nm.

presence of Kondo screening in **Por D**, which is experimentally detected as a resonance at zero bias, as recently also encountered for other open-shell porphyrins.[36,37] Importantly, the experimental results are obtained for longer **1D Por NT** segments (Figure S26).

Furthermore, thanks to a combination of point STS and d*I*/d*V* mapping, we identify frontier orbitals onsets at −0.4 V and 0.3. The experimental d*I*/d*V* maps match well with the calculated ones (Figure S28), ratifying our overall rationalization of the electronic structure. Analogous results are obtained regardless of the length of the fabricated **1D Por NT**, confirming weak electronic coupling between adjacent diradical porphyrin dimer units within the metal-organic 1D polymer. Compared to previous literature where the synthesis of porphyrin nanotapes is introduced,[36,51,52] here we pioneered the fabrication of a quasi-1D nanoarchitecture based on surface-confined coordination chemistry incorporating π-electron magnetic entities.

Conclusion

Herein, we have reported the fabrication of two-fold Au-coordinated porphyrin monomers (**Por HM**), triply-linked porphyrin dimers (**Por HD**), and 1D polymers (**1D Por HNC** and **1D Por HNT**) obtained by on-surface synthesis of

1, a porphyrin precursor bearing two CN moieties, on Au(111)/mica. While all the reaction products are initially obtained as non-magnetic species, they can undergo a singly or doubly hydrogen dissociation process promoted by perturbative bias voltage from the STM tip converting them into Au-coordinated open-shell porphyrin monomers (**Por M**), triply-linked porphyrin dimers (**Por D**), and 1D polymers (**1D Por NC** and **1D Por NT**).

Regarding the role of the coordinated gold adatoms in the magnetic properties of the open-shell porphyrin species, theoretical calculations on **Por M** reveal that the porphyrin unit changes its ground state from triplet to singlet due to the coordination of the terminal carbonitrile moieties to passivated gold adatoms. In contrast, **Por D** features a triplet ground state.

Focusing on the influence of Au-CN coordination in mediating supramolecular magnetic exchange coupling between the coordinated open-shell units, for both **1D Por NC** and **1D Por NT** no magnetic exchange coupling between adjacent units is observed, suggesting negligible magnetic communication across the CN–Au-NC bridge.

In summary, our results illustrate the synergy between on-surface covalent synthesis and coordination chemistry at interfaces to fabricate low-dimensional coordination polymers featuring non-interacting π-electron magnetic porphyrin species. We envision that our contribution will open new avenues in the fields of nanomagnetism and coordination chemistry, particularly in the design of metal-organic nanostructures comprising π-electron magnetic entities.

Supporting Information

The authors have cited additional references within the Supporting Information

Acknowledgements

This project has received funding from MCIN/AEI/10.13039/501100011033 through grants PID2019-108532GB–I00, PID2022-136961NB–I00, PID2020-116490GB–I00, PID2023-151167NB–I00, and TED2021-131255B–C43. IMDEA Nanociencia is appreciative of support from the "Severo Ochoa" Programme for Centers of Excellence in R&D (CEX2020-001039-S). We acknowledge the support from the '(MAD2D-CM)-IMDEA-Nanociencia' and 'Materiales Disruptivos Bidimensionales (2D)" (MAD2D-CM) (UAM1)-MRR Materiales Avanzados' projects funded by Comunidad de Madrid, by the Recovery, Transformation and Resilience Plan, and by NextGenerationEU from the European Union. T.T. also acknowledges the Alexander von Humboldt Foundation (Germany) for the A. v. Humboldt—J.C. Mutis Research Award 2023 (Ref [3].3-1231125—ESP-GSA). We appreciate funding from GACR 23–05486S and the CzechNanoLab Research Infrastructure supported by MEYS CR (LM2023051).

Conflict of Interest

The authors declare no conflict of interest.

Data Availability Statement

The data that support the findings of this study are available from the corresponding author upon reasonable request.

Keywords: π-electron magnetism · coordination chemistry · porphyrinoids · STM

[1] Z. Sun, Q. Ye, C. Chi, J. Wu, *Chem. Soc. Rev.* **2012**, *41*, 7857–7889.
[2] Y. Morita, S. Suzuki, K. Sato, T. Takui, *Nat. Chem.* **2011**, *3*, 197–204.
[3] W. Zeng, J. Wu, *Chem* **2021**, *7*, 358–386.
[4] S. Dong, Z. Li, *J. Mater. Chem. C* **2022**, *10*, 2431–2449.
[5] E. Coronado, A. J. Epstein, *J. Mater. Chem.* **2009**, *19*, 1670–1671.
[6] J. Li, S. Sanz, M. Corso, D. J. Choi, D. Peña, T. Frederiksen, J. I. Pascual, *Nat. Commun.* **2019**, *10*, 200.
[7] S. Mishra, D. Beyer, K. Eimre, J. Liu, R. Berger, O. Gröning, C. A. Pignedoli, K. Müllen, R. Fasel, X. Feng, P. Ruffieux, *J. Am. Chem. Soc.* **2019**, *141*, 10621–10625.
[8] S. Mishra, D. Beyer, K. Eimre, R. Ortiz, J. Fernández-Rossier, R. Berger, O. Gröning, C. A. Pignedoli, R. Fasel, X. Feng, P. Ruffieux, *Angew. Chem. Int. Ed.* **2020**, *59*, 12041–12047.
[9] S. Mishra, K. Xu, K. Eimre, H. Komber, J. Ma, C. A. Pignedoli, R. Fasel, X. Feng, P. Ruffieux, *Nanoscale* **2021**, *13*, 1624–1628.
[10] T. Wang, A. Berdonces-Layunta, N. Friedrich, M. Vilas-Varela, J. P. Calupitan, J. I. Pascual, D. Peña, D. Casanova, M. Corso, D. G. de Oteyza, *J. Am. Chem. Soc.* **2022**, *144*, 4522–4529.
[11] M. Vilas-Varela, F. Romero-Lara, A. Vegliante, J. P. Calupitan, A. Martínez, L. Meyer, U. Uriarte-Amiano, N. Friedrich, D. Wang, F. Schulz, N. E. Koval, M. E. Sandoval-Salinas, D. Casanova, M. Corso, E. Artacho, D. Peña, J. I. Pascual, *Angew. Chem. Int. Ed.* **2023**, *62*, e202307884.
[12] J. P. Calupitan, A. Berdonces-Layunta, F. Aguilar-Galindo, M. Vilas-Varela, D. Peña, D. Casanova, M. Corso, D. G. de Oteyza, T. Wang, *Nano Lett.* **2023**, *23*, 9832–9840.
[13] J. Su, W. Fan, P. Mutombo, X. Peng, S. Song, M. Ondráček, P. Golub, J. Brabec, L. Veis, M. Telychko, P. Jelínek, J. Wu, J. Lu, *Nano Lett.* **2021**, *21*, 861–867.
[14] S. Mishra, D. Beyer, K. Eimre, S. Kezilebieke, R. Berger, O. Gröning, C. A. Pignedoli, K. Müllen, P. Liljeroth, P. Ruffieux, X. Feng, R. Fasel, *Nat. Nanotechnol.* **2020**, *15*, 22–28.
[15] K. Biswas, J. I. Urgel, M. R. Ajayakumar, J. Ma, A. Sánchez-Grande, S. Edalatmanesh, K. Lauwaet, P. Mutombo, J. M. Gallego, R. Miranda, P. Jelínek, X. Feng, D. Écija, *Angew. Chem. Int. Ed.* **2022**, *61*, e202114983.
[16] A. Sánchez-Grande, J. I. Urgel, L. Veis, S. Edalatmanesh, J. Santos, K. Lauwaet, P. Mutombo, J. M. Gallego, J. Brabec, P. Beran, D. Nachtigallová, R. Miranda, N. Martín, P. Jelínek, D. Écija, *J. Phys. Chem. Lett.* **2021**, *12*, 330–336.
[17] E. Turco, S. Mishra, J. Melidonie, K. Eimre, S. Obermann, C. A. Pignedoli, R. Fasel, X. Feng, P. Ruffieux, *J. Phys. Chem. Lett.* **2021**, *12*, 8314–8319.
[18] S. Mishra, J. Melidonie, K. Eimre, S. Obermann, O. Gröning, C. A. Pignedoli, P. Ruffieux, X. Feng, R. Fasel, *Chem. Commun.* **2020**, *56*, 7467–7470.

[19] S. Mishra, X. Yao, Q. Chen, K. Eimre, O. Gröning, R. Ortiz, M. Di Giovannantonio, J. C. Sancho-García, J. Fernández-Rossier, C. A. Pignedoli, K. Müllen, P. Ruffieux, A. Narita, R. Fasel, *Nat. Chem.* **2021**, *13*, 581–586.
[20] K. Biswas, D. Soler, S. Mishra, Q. Chen, X. Yao, A. Sánchez-Grande, K. Eimre, P. Mutombo, C. Martín-Fuentes, K. Lauwaet, J. M. Gallego, P. Ruffieux, C. A. Pignedoli, K. Müllen, R. Miranda, J. I. Urgel, A. Narita, R. Fasel, P. Jelínek, D. Écija, *J. Am. Chem. Soc.* **2023**, *145*, 2968–2974.
[21] W. Zeng, S. Lee, M. Son, M. Ishida, K. Furukawa, P. Hu, Z. Sun, D. Kim, J. Wu, *Chem. Sci.* **2015**, *6*, 2427–2433.
[22] a) H. Zhang, J. Kim, H. Phan, T. Seng Herng, T. Y. Gopalakrishna, W. Zeng, J. Ding, D. Kim, J. Wu, *J. Porphyrins Phthalocyanines* **2020**, *24*, 220–229; b) K. Kato, K. Furukawa, A. Osuka, *Angew. Chem. Int. Ed.* **2018**, *57*, 9491; c) K. Wang, P. Liu, F. Zhang, L. Xu, M. Zhou, A. Nakai, K. Kato, K. Furukawa, T. Tanaka, A. Osuka, J. Song, *Angew. Chem. Int. Ed.* **2021**, *60*, 7002.
[23] a) Q. Sun, L. M. Mateo, R. Robles, P. Ruffieux, N. Lorente, G. Bottari, T. Torres, R. Fasel, *J. Am. Chem. Soc.* **2020**, *142*, 18109–18117; b) Q. Sun, L. M. Mateo, R. Robles, P. Ruffieux, G. Bottari, T. Torres, R. Fasel, N. Lorente, *Adv. Sci.*, **2022**, *9*, 2105906 (1–9).
[24] Q. Sun, L. M. Mateo, R. Robles, N. Lorente, P. Ruffieux, G. Bottari, T. Torres, R. Fasel, *Angew. Chem. Int. Ed.* **2021**, *60*, 16208–16214.
[25] J. V. Barth, G. Costantini, K. Kern, *Nature* **2005**, *437*, 671–679.
[26] L. Dong, Z. Gao, N. Lin, *Prog. Surf. Sci.* **2016**, *91*, 101–135.
[27] D. Écija, J. I. Urgel, A. P. Seitsonen, W. Auwärter, J. V. Barth, *Acc. Chem. Res.* **2018**, *51*, 365–375.
[28] J. I. Urgel, D. Écija, G. Lyu, R. Zhang, C.-A. Palma, W. Auwärter, N. Lin, J. V. Barth, *Nat. Chem.* **2016**, *8*, 657–662.
[29] Q. Shen, H.-Y. Gao, H. Fuchs, *Nano Today* **2017**, *13*, 77–96.
[30] Q. Sun, R. Zhang, J. Qiu, R. Liu, W. Xu, *Adv. Mater.* **2018**, *30*, 1705630.
[31] S. Clair, D. G. de Oteyza, *Chem. Rev.* **2019**, *119*, 4717–4776.
[32] S. Mishra, G. Catarina, F. Wu, R. Ortiz, D. Jacob, K. Eimre, J. Ma, C. A. Pignedoli, X. Feng, P. Ruffieux, J. Fernández-Rossier, R. Fasel, *Nature* **2021**, *598*, 287–292.
[33] Y. Zhao, K. Jiang, C. Li, Y. Liu, G. Zhu, M. Pizzochero, E. Kaxiras, D. Guan, Y. Li, H. Zheng, C. Liu, J. Jia, M. Qin, X. Zhuang, S. Wang, *Nat. Chem.* **2023**, *15*, 53–60.
[34] J. Hieulle, S. Castro, N. Friedrich, A. Vegliante, F. R. Lara, S. Sanz, D. Rey, M. Corso, T. Frederiksen, J. I. Pascual, D. Peña, *Angew. Chem. Int. Ed.* **2021**, *60*, 25224–25229.
[35] Y. Zhao, K. Jiang, C. Li, Y. Liu, C. Xu, W. Zheng, D. Guan, Y. Li, H. Zheng, C. Liu, W. Luo, J. Jia, X. Zhuang, S. Wang, *J. Am. Chem. Soc.* **2020**, *142*, 18532–18540.
[36] Q. Sun, L. M. Mateo, R. Robles, N. Lorente, P. Ruffieux, G. Bottari, T. Torres, R. Fasel, *Angew. Chem. Int. Ed.* **2021**, *60*, 16208–16214.
[37] K. Biswas, M. Urbani, A. Sánchez-Grande, D. Soler-Polo, K. Lauwaet, A. Matěj, P. Mutombo, L. Veis, J. Brabec, K. Pernal, J. M. Gallego, R. Miranda, D. Écija, P. Jelínek, T. Torres, J. I. Urgel, *J. Am. Chem. Soc.* **2022**, *144*, 12725–12731.
[38] A. Wiengarten, K. Seufert, W. Auwärter, D. Ecija, K. Diller, F. Allegretti, F. Bischoff, S. Fischer, D. A. Duncan, A. C. Papageorgiou, F. Klappenberger, R. G. Acres, T. H. Ngo, J. V. Barth, *J. Am. Chem. Soc.* **2014**, *136*, 9346–9354.
[39] L. Yan, I. Pohjavirta, B. Alldritt, P. Liljeroth, *ChemPhysChem* **2019**, *20*, 2297–2300.
[40] T. A. Pham, F. Song, M. N. Alberti, M.-T. Nguyen, N. Trapp, C. Thilgen, F. Diederich, M. Stöhr, *Chem. Commun.* **2015**, *51*, 14473–14476.
[41] J. C. Moreno-López, A. Pérez Paz, S. Gottardi, L. Solianyk, J. Li, L. Monjas, A. K. H. Hirsch, D. J. Mowbray, M. Stöhr, *J. Phys. Chem. C* **2021**, *125*, 9847–9854.
[42] Z. Li, M. Smeu, M. A. Ratner, E. Borguet, *J. Phys. Chem. C* **2013**, *117*, 14890–14898.
[43] D. G. de Oteyza, T. Frederiksen, *J. Phys. Condens. Matter* **2022**, *34*, 443001.
[44] V. Blum, R. Gehrke, F. Hanke, P. Havu, V. Havu, X. Ren, K. Reuter, M. Scheffler, *Comput. Phys. Commun.* **2009**, *180*, 2175–2196.
[45] B. O. Roos, P. R. Taylor, P. E. M. Sigbahn, *Chem. Phys.* **1980**, *48*, 157–173.
[46] Y. Guo, K. Sivalingam, E. F. Valeev, F. Neese, *J. Chem. Phys.* **2016**, *144*, 094111.
[47] F. Neese, *WIREs Comput. Mol. Sci.* **2012**, *2*, 73–78.
[48] R. L. Martin, *J. Chem. Phys.* **2003**, *118*, 4775–4777.
[49] O. Krejčí, P. Hapala, M. Ondráček, P. Jelínek, *Phys. Rev. B* **2017**, *95*, 045407.
[50] A. Calvo-Fernandez, M. Kumar, D. Soler-Polo, D. Eiguren, M. Blanco-Rey, P. Jelínek, *Phys. Rev. B* **2024**, *110*, 165113.
[51] Z. Chen, J.-R. Deng, S. Hou, X. Bian, J. L. Swett, Q. Wu, J. Baugh, L. Bogani, G. A. D. Briggs, J. A. Mol, C. J. Lambert, H. L. Anderson, J. O. Thomas, *J. Am. Chem. Soc.* **2023**, *145*, 15265–15274.
[52] A. Tsuda, A. Osuka, *Science* **2001**, *293*, 79–82.

Manuscript received: October 23, 2024
Accepted manuscript online: December 6, 2024
Version of record online: ■■, ■■

Research Article

Porphyrinoids

M. Tenorio,* M. Lozano, L. Cerna, M. Martínez García, M. Urbani, K. Lauwaet, K. Biswas, D. Soler-Polo, S. K. Mathialagan, S. O. Parreiras, J. M. Gallego, R. Miranda, J. I. Urgel, T. Torres,* P. Jelínek,* G. Bottari,* D. Écija* _____ **e202420572**

Coordinative Self-assembly of π-Electron Magnetic Porphyrins

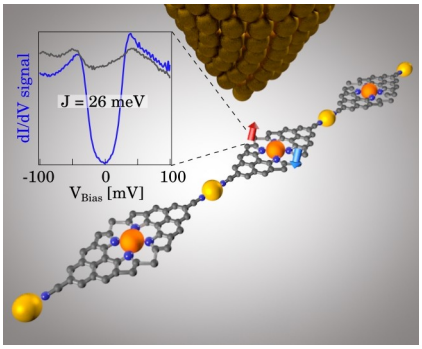

Gold-coordinated polymers of π-extended porphyrins were fabricated by on-surface synthesis and coordination chemistry methods. Each porphyrinoid monomer features antiferromagnetic coupling and no interaction between nearest neighbors within the polymer backbone, behaving as a single magnetic entity.